Journal of Power Sources 241 (2013) 728–735

Contents lists available at SciVerse ScienceDirect

Journal of Power Sources

journal homepage: www.elsevier.com/locate/jpowsour

Short communication

Structure and electrochemical activity of WO_x-supported PtRu catalyst using three-dimensionally ordered macroporous WO_3 as the template

Qi Wang [a,b,*], Guoxiong Wang [b], Keisuke Sasaki [b], Tatsuya Takeguchi [b,**], Toshiro Yamanaka [b], Masahiro Sadakane [b], Wataru Ueda [b]

[a] Liaoning Key Materials Laboratory for Railway, School of Materials Science and Engineering, Dalian Jiaotong University, Dalian 116028, China
[b] Catalysis Research Center, Hokkaido University, Sapporo 001-0021, Japan

HIGHLIGHTS

- Three-dimensionally ordered macroporous WO_3 is used as a template.
- PtRu/WO_x catalyst with an ordered porous structure is prepared.
- The WO_x improves metallic Pt proportion in the PtRu/WO_x catalyst greatly.
- The WO_x promotes CO_{ads} and methanol electro-oxidation on the PtRu/WO_x catalyst.
- The porous structure benefits mass transport of methanol to the catalyst surface.

ARTICLE INFO

Article history:
Received 15 February 2013
Received in revised form
4 June 2013
Accepted 4 June 2013
Available online 14 June 2013

Keywords:
Three-dimensionally ordered macroporous tungsten trioxide
Template
Porous structure
PtRu catalyst
Methanol oxidation

ABSTRACT

PtRu/WO_x catalyst is prepared in a polyol process with three-dimensionally ordered macroporous (3DOM) WO_3 as the template in combination with an ammonia-leaching treatment. The morphology, composition and structure of the prepared catalysts are characterized by scanning transmission electron microscopy, energy dispersion X-ray spectroscopy, N_2 adsorption, X-ray photoelectron spectroscopy and X-ray diffraction. The electrochemical activities are evaluated by linear sweep voltammetry, cyclic voltammetry, and chronoamperometry measurements in combination with *in situ* IR reflection absorption spectroscopy (IRRAS). The composition and particle size of the PtRu/WO_x catalyst are similar to those of the PtRu catalyst prepared without the 3DOM WO_x template, and both of the catalysts have a uniform element distribution, however, the PtRu/WO_x catalyst has a more porous structure and greater metallic Pt proportion due to the support role of the residual WO_x template and the interaction between WO_x and PtRu nanoparticles. Electrochemical and *in situ* IRRAS measurements indicate that the PtRu/WO_x catalyst has a greater electro-catalytic activity for methanol oxidation than the PtRu catalyst due to the assisting catalytic role of WO_x and mass transport benefit of the porous structure.

1. Introduction

Direct methanol fuel cells (DMFCs) have been considered as a suitable candidate for portable power sources due to their high theoretical energy density and mild operating conditions [1,2]. Compared with the electro-oxidation of H_2 in the anode of polymer electrolyte fuel cells (PEFCs), the electro-oxidation of methanol in the anode of DMFCs suffers from slow kinetics, which results in a poor performance [2]. In order to mitigate this problem, unsupported PtRu black catalyst with a high loading is widely used in the anode catalyst layer [3–5]. It is well known that unsupported Pt-based catalyst is prone to agglomerate during the catalyst and electrode preparation process, which decreases the metal utilization dramatically [3,6].

Various preparation methods have been developed to improve the dispersion of metal nanoparticles [7,8]. As an effective route, templates are usually used to prepare unsupported Pt-based catalyst with ordered structures and a great specific surface area [7–16]. Different ordered structures such as nanowire, nanotube, etc. have been reported using track-etched polycarbonate membrane, anodic

* Corresponding author. Liaoning Key Materials Laboratory for Railway, School of Materials Science and Engineering, Dalian Jiaotong University, Dalian 116028, China.
** Corresponding author. Catalysis Research Center, Hokkaido University, Sapporo 001-0021, Japan.
E-mail addresses: q.wang0501@gmail.com (Q. Wang), takeguch@cat.hokudai.ac.jp (T. Takeguchi).

0378-7753/$ – see front matter © 2013 Elsevier B.V. All rights reserved.
http://dx.doi.org/10.1016/j.jpowsour.2013.06.020

aluminum oxide membrane and Ag wire as templates [10–12]. However, the used templates are usually negative or inert to the electro-catalytic reaction, and the complete removal of the template is vital for obtaining a superior electro-catalytic activity [7,8]. Due to the weak interaction between the nanoparticles, there are some questions as to whether the ordered structures of the catalysts were destroyed and particle agglomeration occurred after the template was completely removed [7,8]. Therefore, there is a great challenge for preparing unsupported Pt-based catalysts with an ordered structure.

It is reported that various metal oxides such as SnO_x, MoO_x and WO_x showed remarkably assisting electro-catalytic role for CO and methanol oxidation [17–24]. The strong interaction between Pt and metal oxides was usually considered as the dominant factor for greatly promoting the electro-catalytic activity [17–24]. In order to obtain more interfaces between the Pt and metal oxides, the Pt-based metal nanoparticles were deposited on the metal oxide instead of carbon support [25–28]. However, carbon black was essential to be mixed physically in the catalyst ink for improving the electronic conductivity during the electrochemical measurements [27,28]. In addition, the surface area of the used metal oxide was not great enough for supporting a high loading of Pt-based nanoparticles due to particle agglomeration. Three-dimensionally ordered macroporous (3DOM) structures possessed a great specific surface area and low mass transport loss, and some metal oxides with 3DOM structure have been synthesized successfully [29–31]. For example, the 3DOM WO_3-supported Pt demonstrated enhanced photo–catalytic activity for acetic acid decomposition under visible light [30,31]. In view of the great specific surface area of 3DOM WO_3 and assisting electro-catalytic role of WO_x for CO and methanol oxidation [23–28,30,31], we have examined the use of 3DOM WO_3 as a template for supporting PtRu nanoparticles prepared in a polyol process, and then a high PtRu loading was obtained in the PtRu/WO_x catalyst by dissolving majority of the 3DOM WO_3 in ammonia solution, thus carbon black is not necessary to be added into the catalyst ink during the electrochemical measurements since the PtRu nanoparticles could form the electronic conducting pathway. The morphology, composition and structure of the prepared catalysts were characterized by scanning transmission electron microscopy (STEM), energy dispersion X-ray spectroscopy (EDX), N_2 adsorption, X-ray photoelectron spectroscopy (XPS) and X-ray diffraction (XRD). Conventional electrochemical measurements, in combination with *in situ* infrared reflection absorption spectroscopy (IRRAS), were conducted to evaluate the electro-catalytic activity for CO_{ads} and methanol oxidation on the prepared catalysts.

2. Experimental

2.1. Catalyst preparation

3DOM WO_3 was synthesized using ammonium metatungstate as the precursor and poly methyl methacrylate (PMMA) colloidal crystals as the template, and the detailed preparation procedures were described elsewhere [30,31]. PtRu colloid was prepared in a polyol process as described below: calculated amounts of $H_2PtCl_6 \cdot 6H_2O$ and $RuCl_3 \cdot xH_2O$ (the nominal atomic ratio of Pt to Ru of 1:1) were dissolved in ethylene glycol in a three-necked flask to form a brown solution with a concentration of 2 mg (Pt + Ru) mL^{-1}. Then the pH value of the solution was increased to about 13 by adding 1 M NaOH solution. The solution was heated up to 170 °C at a rate of 10 °C min^{-1} and kept at that temperature for 4 h, and then the PtRu colloid solution was cooled down to room temperature. The 3 DOM WO_3-supported PtRu catalyst was prepared as follows: the pH value of the PtRu colloid solution was adjusted to about 7 with HCl solution, and the 3DOM WO_3 was added into to the PtRu colloid solution (the nominal weight ratio of 3DOM WO_3 to PtRu of 1:1), then the pH value of the PtRu colloid solution was further decreased to about 2. The mixture was heated to 90 °C and kept at that temperature for 24 h, the obtained sample was centrifuged and denoted as PtRu/3DOM WO_3. Then the solid was immersed in 15 wt.% $NH_3 \cdot H_2O$ and stirred for about 48 h at room temperature to dissolve majority of the 3DOM WO_3 template. Finally, the sample was centrifuged and washed with de-ionized water for several cycles to remove excess ammonia in the catalyst, and the catalyst was dried and denoted as PtRu/WO_x catalyst. For comparison, PtRu colloid was deposited without adding the 3DOM WO_3 template in the same manner as described above and denoted as PtRu catalyst.

2.2. Physicochemical characterization

Catalyst morphology and element distribution of the catalysts were investigated by a STEM (Hitachi HD-2000) with EDAX Genesis System 4000 at 200 kV and 30 μA. N_2 adsorption of the catalysts was carried out using an ASAP2020 Micromeritics Instrument at −196 °C. Specific surface areas of the catalysts were calculated by the Brunauer-Emmett-Teller (BET) equation. XPS measurements were carried out using a JEOL JPS-9010MC spectrometer with a Mg Kα radiation source. The Pt (4f), Ru (3p) and W (4f) signals were

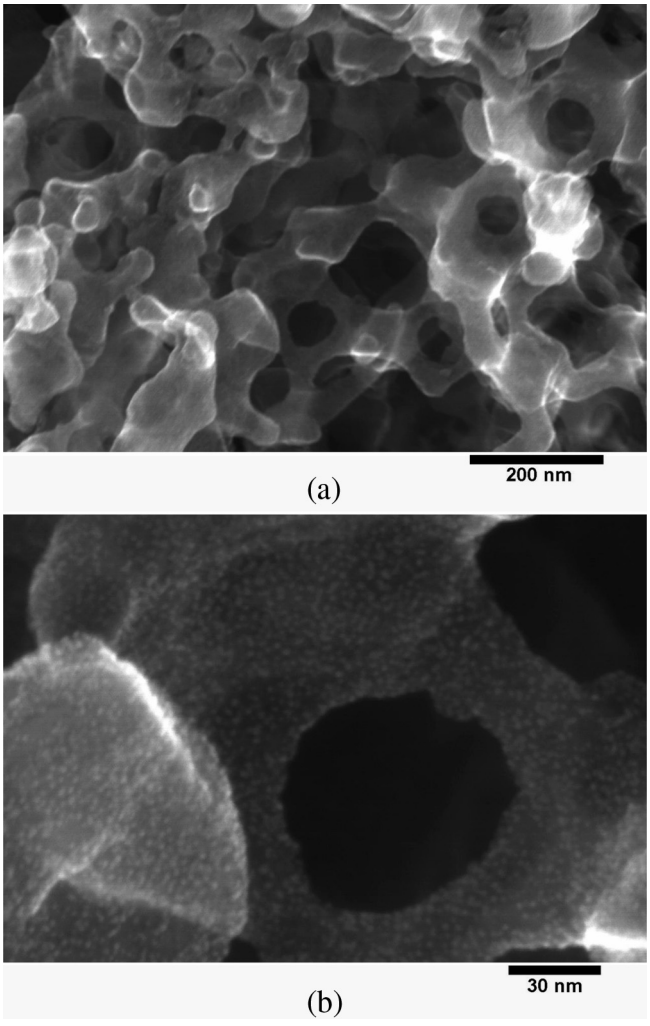

Fig. 1. SEM images of PtRu/3DOM WO_3 catalyst (a), (b).

collected. The position of the C (1s) peak, that is, 284.2 eV for the JEOL JPS-9010MC spectrometer, was used to correct the binding energies of the PtRu/WO_x and PtRu catalysts. XRD patterns of the catalysts were recorded with a Powder X-ray diffractometer (RIGAKU, RINT 2000) using Cu Kα radiation with a Ni filter. The tube current was 20 mA with a tube voltage of 40 kV.

2.3. Electrochemical measurements

Electrochemical measurements were carried out in a 250 mL three-electrode cell (HR200, Hokuto Denko Corp.) at 25 °C. A commercial glassy carbon (GC) electrode (HR2-D1-GC-5, 5 mm in diameter, 0.196 cm^2, Hokuto Denko Corp.) covered by the PtRu/WO_x or PtRu catalyst with Nafion ionomer as a binder, Pt-wire electrode (Hokuto Denko Corp.) and a saturated calomel electrode (SCE, Hokuto Denko Corp.) were used as a working electrode, a counter electrode and a reference electrode, respectively. The potential of the working electrode was controlled by an Iviumstat Electrochemical Interface System (Ivium Technologies B.V.). Six mg of the catalyst was dispersed in a mixture of 2 mL water, 3 mL ethanol and 50 μL Nafion solution (5 wt.%, Aldrich) with ultrasonic stirring to form a homogenous ink [32]. The catalyst layer was prepared by dropping 10 μL of the ink onto a GC disk electrode by a microsyringe and drying at room temperature. All potential values in this paper are referred to a reversible hydrogen electrode (RHE). For CO stripping voltammetry measurements, pure CO was supplied into the electrolyte solution (0.1 M $HClO_4$) for 20 min at a fixed potential of 0.05 V, and then high-purity Ar was bubbled for 30 min to remove the CO dissolved in the electrolyte solution. The current–potential cycles were obtained from 0.05 to 1.2 V at a scan rate of 10 mV s^{-1}. Cyclic voltammetries (CVs) of methanol electro-oxidation were measured in a potential range of 0–1.042 V in 0.1 M $HClO_4$ + 0.5 M CH_3OH solution saturated with high-purity Ar gas, and the scan rate was 20 mV s^{-1}. Linear sweep voltammetries (LSVs) of methanol electro-oxidation were recorded from 0 to 0.6 V at a scan rate of 1 mV s^{-1}. The chronoamperometry (CA) curves were obtained by polarizing the electrode at 0.55 V for 900 s in the above-mentioned electrolyte solution.

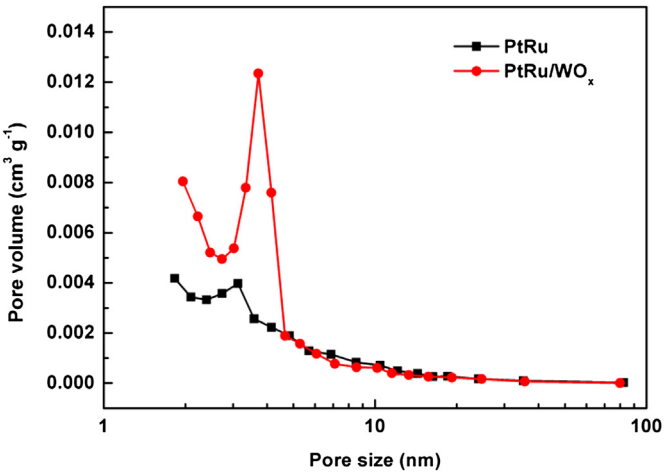

Fig. 3. Pore size distribution of PtRu/WO_x and PtRu catalysts.

The *in situ* IRRAS measurements were carried out in a home-made PTFE cell with a CaF_2 optical window using a JASCO FT/IR-6100 spectrometer equipped with a TGS detector [33]. A gold disk (10 mm in diameter) was used as an electrode substrate for IRRAS measurements, which is inert to methanol electro-oxidation. The catalyst layers were deposited on the gold electrode surface with the same method as described for the electrochemical measurements of CO_{ads} and methanol oxidation. Then the electrode was pushed onto the CaF_2 prism window with the thin-layer geometry to reduce the IR absorption by aqueous solution. The *in situ* IR spectra were recorded with a scan rate of 0.25 mV s^{-1}, and 25

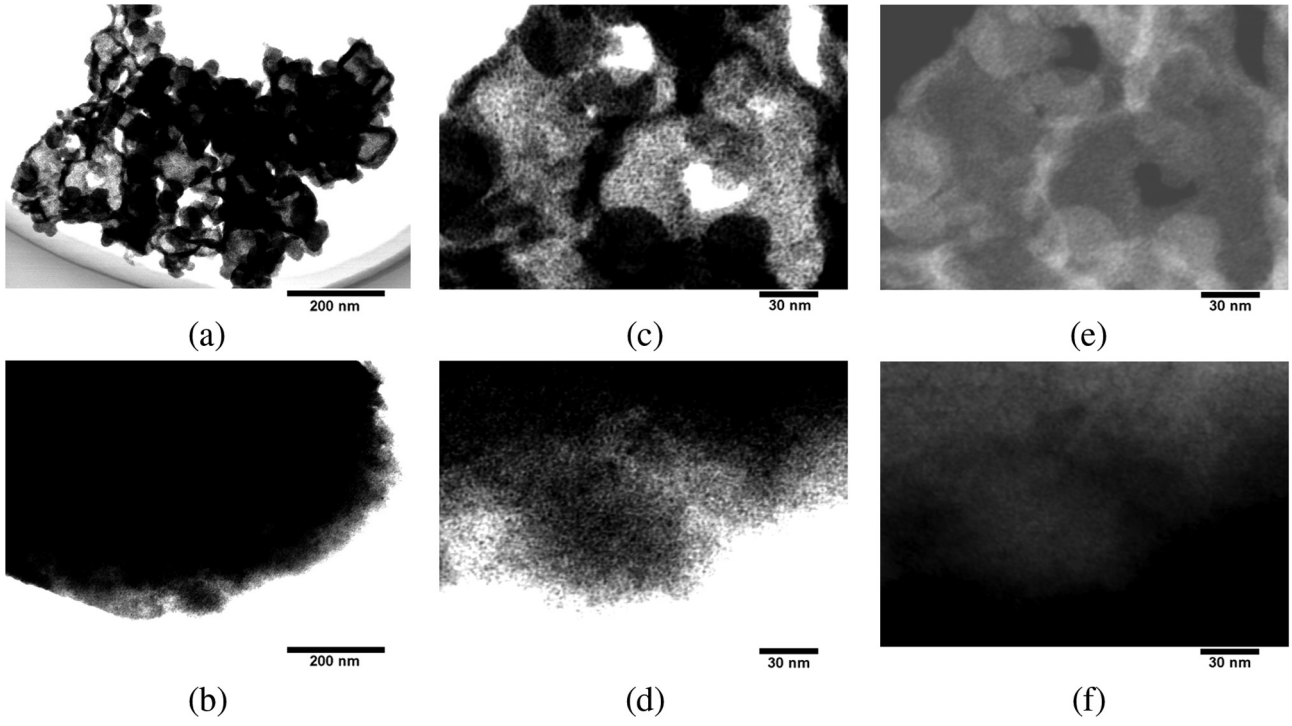

Fig. 2. STEM images of PtRu/WO_x (a), (c), (e) and PtRu catalysts (b), (d), (f).

interferograms were co-added to each spectrum. All the IR spectra were normalized to a reference spectrum recorded at 0.0 V in 0.1 M $HClO_4$ + 0.5 M CH_3OH solution in unit of absorbance.

3. Results and discussion

3.1. STEM, EDX and N_2 adsorption characterization

Fig. 1 (a) and (b) shows SEM images of the PtRu/3DOM WO_3 prior to immersing in ammonia solution. In order to prohibit the dissolution of 3DOM WO_3 in alkaline solution, the pH value of the prepared PtRu colloid was decreased to about 7 before adding 3DOM WO_3 into the PtRu colloid solution. It can be observed that the structure of the 3DOM WO_3 template was maintained and the PtRu nanoparticles were uniformly deposited on the walls of the 3DOM WO_3. Then the PtRu/3DOM WO_3 was immersed in ammonia solution to remove majority of the 3DOM WO_3.

Fig. 2 shows STEM images of the PtRu/WO_x and PtRu catalysts. It can be observed from Fig. 2 (a), (c) and (e) that there are macro pores in the PtRu/WO_x catalyst, which was replicated from the 3DOM WO_3 template. The space between the PtRu nanoparticles consists of pores with a size of 2 ~ 5 nm, which was probably induced by the leaching of the 3DOM WO_3 template out to the ammonia solution. After the leaching, the ordered structure was still maintained in the PtRu/WO_x catalyst. The porous structure in the PtRu/WO_x catalyst is expected to be beneficial for the reactant access to the PtRu nanoparticles [34]. Fig. 2 (b) shows STEM image of the PtRu catalyst. The particle size of the PtRu catalyst is similar to that of the PtRu/WO_x catalyst, however, the PtRu nanoparticles have a severe agglomeration and much less porous structure. As shown in Fig. 2 (d) and (f), the space between the PtRu nanoparticles in the PtRu catalyst is smaller than that in the PtRu/WO_x catalyst. The specific surface area of the PtRu/WO_x and PtRu catalysts was measured to be 46.7 and 19.2 $m^2\ g^{-1}$, respectively. Fig. 3 shows pore size distribution of the PtRu/WO_x and PtRu catalysts. The pore with a size of 2 ~ 5 nm is considered to be attributed from the space between PtRu nanoparticles, and the pore volume of the PtRu/WO_x catalyst in this region is much greater than that of the PtRu catalyst, suggesting that PtRu nanoparticles in the PtRu/WO_x catalyst are well dispersed, in agreement with the results shown in Fig. 2. Therefore, it is speculated that a critical step for preventing particle agglomeration is the deposition of PtRu nanoparticles. During the polyol process, Pt and Ru precursors were reduced by ethylene glycol to form PtRu colloid, which was stabilized by the glycolate, an oxidation product of ethylene glycol in alkaline medium. After adding diluted HCl solution, the pH value decreased to about 2, and the stability of the PtRu colloid was destroyed by decreasing the concentration of the colloid stabilizer-glycolate [5,6,33]. With using the 3DOM WO_3 template, the PtRu nanoparticles were deposited onto the 3DOM WO_3, prohibiting particle agglomeration. In the case of that without using the 3DOM WO_3 template, the PtRu particles deposited from the suspended phase and agglomerated together. Therefore, the use of 3DOM WO_3 template greatly improved the particle dispersion, and after dissolving majority of the template, the particles did not agglomerate any more.

Elemental mappings of the PtRu/WO_x and PtRu catalysts were analyzed using EDX, as shown in Fig. 4. For the PtRu/WO_x and PtRu catalysts, the mapping image of Pt element coincides with that of Ru element, suggesting a uniform distribution of Pt and Ru in the catalysts. In addition, the mapping image of W element in the PtRu/WO_x catalyst was also detected, as shown in Fig. 4 (a). The mapping image of W element also coincides with those of Pt and Ru elements, but the intensity is much lower than those of Pt and Ru elements, suggesting that majority of 3DOM WO_3 was dissolved in the ammonia solution.

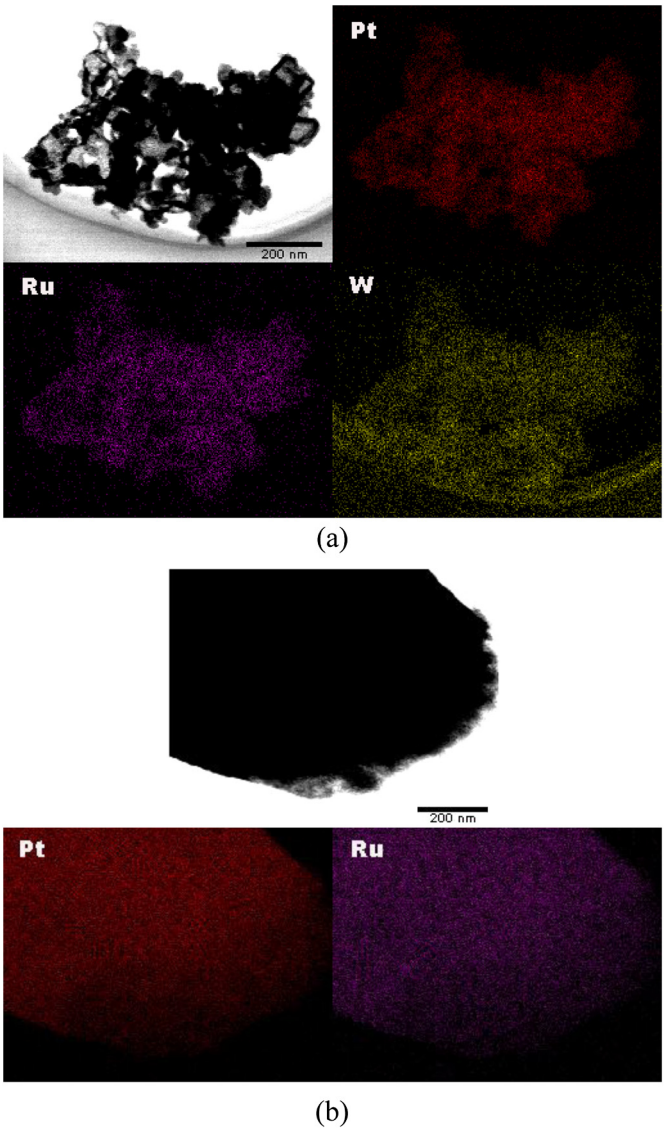

Fig. 4. STEM image and elemental mappings of PtRu/WO_x (a) and PtRu (b) catalysts.

3.2. XPS and XRD characterization

XPS was used to analyze the oxidation state of Pt, Ru and W in the catalysts. Fig. 5 shows Pt 4f spectra of the PtRu/WO_x and PtRu catalysts. The Pt $4f_{7/2}$ XPS line is fitted with a convolution of three peaks corresponding to three different oxidation states of Pt. The results obtained by deconvoluting the XPS spectra are summarized in Table 1. The first peak (71.1 eV) is assigned to the reduced Pt (0) species, whereas the second peak (72.9 eV) is associated with oxidized Pt atoms from PtO species. The third peak (74.9 eV) is assigned to PtO_2 species [35]. As listed in Table 1, the proportion of metallic Pt in the PtRu/WO_x catalyst is 68.6% of the total Pt, while the proportion of metallic Pt in the PtRu catalyst is 37.9% of the total Pt, suggesting that the oxidation state of platinum was greatly modified by the presence of WO_x species [36]. In addition, there is also a slightly greater proportion of metallic Ru in the PtRu/WO_x catalyst than that in the PtRu catalyst. While there are different oxidation states of W in the PtRu/WO_x catalyst, and only 28.3% of W

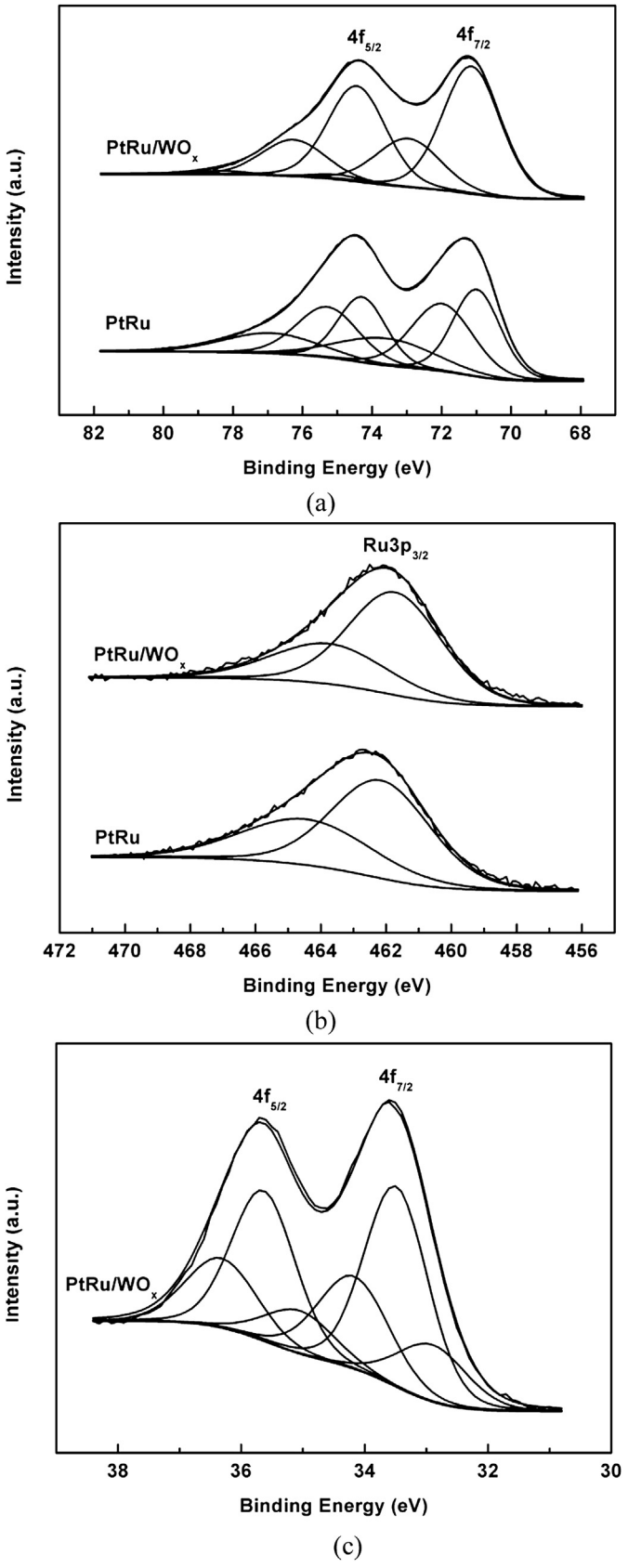

Fig. 5. Pt 4f (a) and Ru 3p (b) signals in the XPS spectra of $PtRu/WO_x$ and PtRu catalysts, and W 4f (c) signal in the XPS spectra of $PtRu/WO_x$ catalyst.

Table 1
XPS analysis results obtained by curve fitting in Fig. 5.

Catalyst	Species	Binding energy (eV)	Peak half width (eV)	Assignment	Atomic ratio (%)
$PtRu/WO_x$	Pt $4f_{7/2}$	71.1	1.9	Pt	68.6
		72.9	2.2	PtO	29.1
		74.9	1.7	PtO_2	2.3
	Ru $3p_{3/2}$	461.7	3.3	Ru	67.2
		463.7	4.2	RuO_2	32.8
	W $4f_{7/2}$	32.9	1.3	WO_2	17.1
		33.5	1.2	W_2O_5, HWO_3	54.6
		34.2	1.4	WO_3	28.3
PtRu	Pt $4f_{7/2}$	71.0	1.6	Pt	37.9
		72.0	2.1	PtO	38.2
		73.6	3.3	PtO_2	23.9
	Ru $3p_{3/2}$	462.1	3.6	Ru	62.0
		464.5	4.7	RuO_2	38.0

species is assigned to WO_3, suggesting that electron transfer occurred from WO_x to Pt, therefore, the Pt surface contains significantly less surface oxides [36].

The surface composition of the PtRu catalyst was estimated from the XPS spectra by using peak areas normalized on the basis of sensitivity factors, and the results are listed in Table 2. The $PtRu/WO_x$ and PtRu catalysts have a similar Pt/Ru surface atomic ratio. The atomic ratio of the catalysts was also measured by EDX. The EDX results, measured randomly at three positions in the catalysts are also summarized in Table 2. The composition at different positions is similar, suggesting a uniform distribution of different elements in the catalysts. The Pt/Ru atomic ratio measured by EDX is greater than the nominal value of 1 in the precursors of Pt and Ru, which is probably due to that the Ru precursor was incompletely reduced by ethylene glycol or that the Ru particles were incompletely deposited [6]. The ratio measured by XPS is greater than that from the EDX results, indicating that the polyol-synthesized PtRu catalyst is Pt rich on the catalyst surface, which is ascribed to that the surface tension of Pt is lower than that of Ru [37,38]. Both of the XPS and EDX results indicate that there is about 4.0 at.% W species in the $PtRu/WO_x$ catalyst.

XRD patterns of the $PtRu/WO_x$ and PtRu catalysts are shown in Fig. 6. All of the diffraction peaks are weak, and only the Pt (111) diffraction peak can be clearly observed, indicative of poor crystalline structures in the $PtRu/WO_x$ and PtRu catalysts. Although only a part of PtRu alloy formation occurred in the polyol process [6], the diffraction peaks of Ru are still not be observed, which is probably due to that the Ru species is amorphous in the $PtRu/WO_x$ and PtRu catalysts [6,36]. Because there is only a small amount of WO_x in the $PtRu/WO_x$ catalyst, the diffraction peaks of WO_x cannot be observed.

3.3. Electrochemical measurements of CO_{ads} and methanol oxidation

Fig. 7 shows CO stripping voltammetries of the $PtRu/WO_x$ and PtRu catalysts. For the PtRu catalyst, CO_{ads} was electro-oxidized in a

Table 2
Composition and Pt/Ru atomic ratio in the $PtRu/WO_x$ and PtRu catalysts.

Catalyst	Measurement method		Composition (atomic ratio %)			Pt/Ru atomic ratio
			Pt	Ru	W	
$PtRu/WO_x$	XPS		63.5	32.6	3.9	1.9
	EDX	Position 1	56.6	39.1	4.3	1.4
		Position 2	57.0	39.1	3.9	1.5
		Position 3	57.0	39.0	4.0	1.5
PtRu	XPS		65.6	34.4	/	1.9
	EDX	Position 1	58.6	41.4	/	1.4
		Position 2	59.2	40.8	/	1.5
		Position 3	56.2	43.8	/	1.3

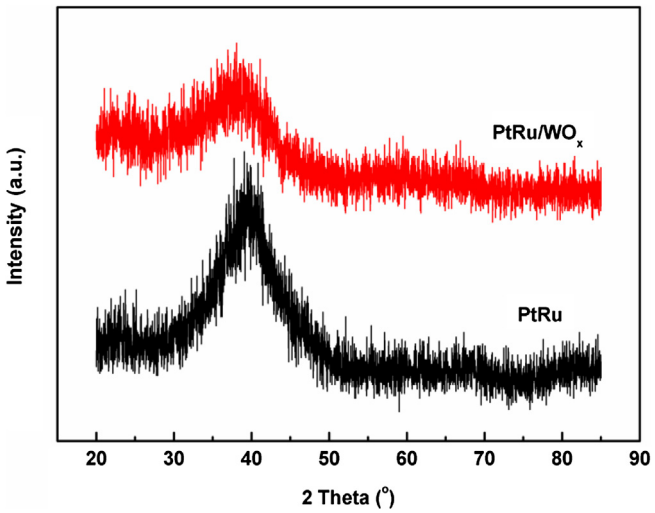

Fig. 6. XRD patterns of PtRu/WO_x and PtRu catalysts.

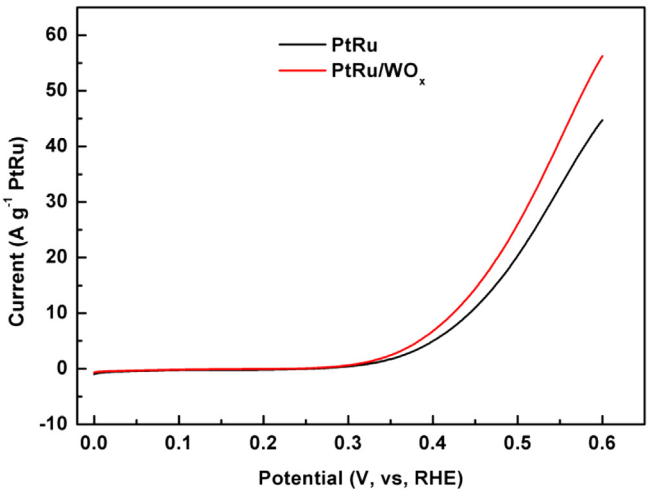

Fig. 8. Linear sweep voltammetries of methanol electro-oxidation on PtRu/WO_x and PtRu catalysts in 0.1 M $HClO_4$ + 0.5 M CH_3OH at 25 °C. Scan rate: 1 mV s^{-1}.

relatively sharp stripping peak centered at 0.496 V, and the peak potential is slightly lower than that for CO_{ads} electro-oxidation on the PtRu/C catalyst prepared with the same method [19]. For the PtRu/WO_x catalyst, both of the onset and peak potentials for CO_{ads} electro-oxidation show obviously negative shifts, indicating that the CO_{ads} electro-oxidation activity was promoted by the interaction between PtRu and residual WO_x, in agreement with the reported result [24]. In addition, it can be observed from the second scan that the under-potentially deposited hydrogen (H_{upd}) desorption current on the PtRu/WO_x catalyst is lower than that on the PtRu catalyst. In the PtRu/WO_x catalyst, there are abundant interfaces between PtRu and WO_x, hence adsorbed hydrogen on the PtRu surface could be conveniently spilled over onto the WO_x surface, promoting the formation of hydrogen tungsten bronze [27].

To validate the electro-catalytic activity and stability for methanol oxidation on the PtRu/WO_x and PtRu catalysts, LSV, CV and CA curves were recorded and presented in Figs. 8–10. The current on the PtRu/WO_x catalyst is greater than that on the PtRu catalyst in both of the activity and stability measurements. It should be noted that the peak current of methanol electro-oxidation on the PtRu/

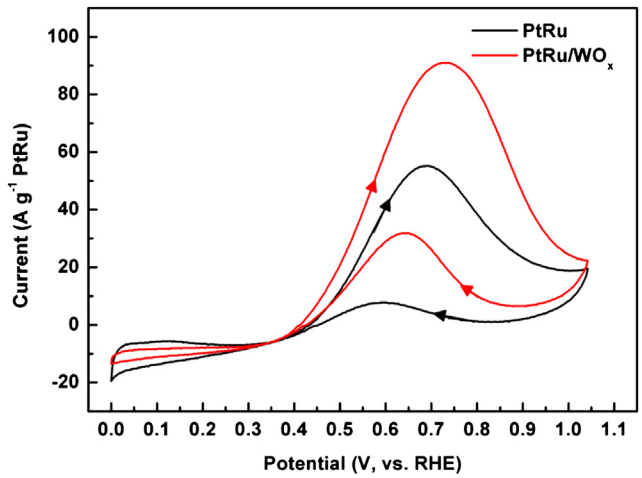

Fig. 9. Cyclic voltammetries of methanol electro-oxidation on PtRu/WO_x and PtRu catalysts in 0.1 M $HClO_4$ + 0.5 M CH_3OH at 25 °C. Scan rate: 20 mV s^{-1}.

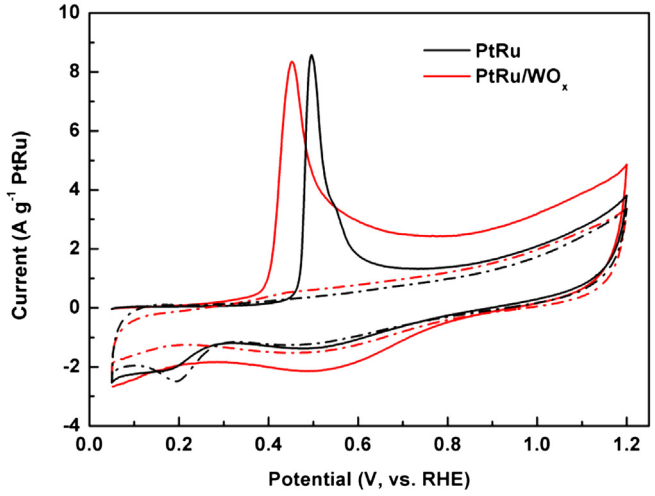

Fig. 7. CO stripping voltammetries on PtRu/WO_x and PtRu catalyst in 0.1 M $HClO_4$ at 25 °C. Scan rate: 10 mV s^{-1}. Solid line shows the first scan and dash dot line shows the second scan.

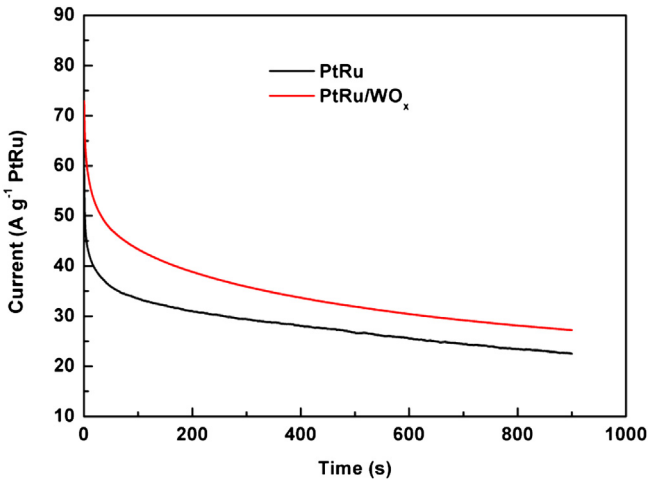

Fig. 10. Chronoamperometry curves of PtRu/WO_x and PtRu catalysts at 0.55 V in 0.1 M $HClO_4$ + 0.5 M CH_3OH at 25 °C.

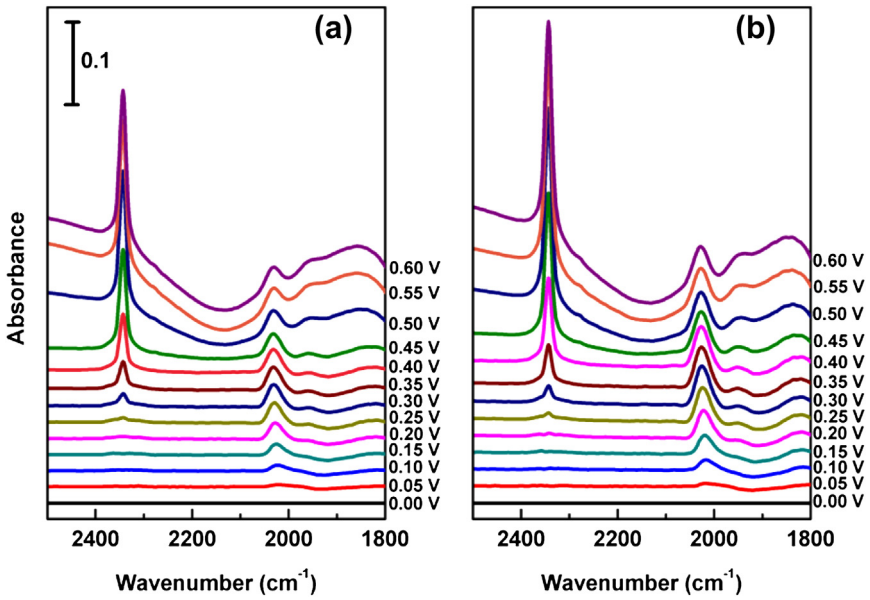

Fig. 11. *In situ* IRRAS spectra of PtRu (a) and PtRu/WO_x (b) catalysts deposited on a gold substrate surface observed in 0.1 M $HClO_4$ + 0.5 M CH_3OH at 25 °C. Potentials are indicated on the right side of each spectrum, reference spectrum was recorded at 0.0 V.

WO_x catalyst in Fig. 9 is much greater than that on the PtRu catalyst, while both catalysts have similar particle size and surface composition, so the much difference in peak current could be ascribed to the mass transport of methanol from the electrolyte solution to the catalyst surface, suggesting that the porous structure in the PtRu/WO_x catalyst was more beneficial for mass transport than the agglomerated structure in the PtRu catalyst.

3.4. *In situ* IRRAS measurement

In situ IRRAS measurement was carried out to understand the molecular structures on the surface of the PtRu/WO_x and PtRu catalysts during the methanol electro-oxidation reaction. Fig. 11 shows *in situ* IR spectra obtained from the PtRu/WO_x and PtRu catalysts surface in 0.1 M $HClO_4$ + 0.5 M CH_3OH solution, respectively in the potential region between 0.0 and 0.6 V. As shown in Fig. 11 (a), a peak at 2026 cm^{-1} with a small shoulder at 1950 cm^{-1} is clearly observed above 0.10 V, and a broad band can also be identified at 1828 cm^{-1}. The peaks at 2026 cm^{-1} and 1828 cm^{-1} are assigned to linearly adsorbed CO (CO_L) and bridge adsorbed CO (CO_B) on the Pt sites [39–41]. The small shoulder at 1950 cm^{-1} can be attributed to CO adsorbed on Ru sites (CO_{Ru}) [39–41], which was probably due to that CO_{ads} migrated from Pt sites to Ru sites during methanol electro-oxidation [42]. Fig. 12 shows the intensities of CO_L on the PtRu/WO_x and PtRu catalysts at different potentials. The intensity of CO_L on the PtRu/WO_x catalyst is greater than that on the PtRu catalyst, indicating that methanol dehydrogenation reaction occurred more easily on the PtRu/WO_x catalyst [25,27]. The residual WO_x in the PtRu/WO_x catalyst was probably converted into tungsten bronzes compound, and the hydrogen spillover from the Pt surface to the surface of hydrogen tungsten bronze could free these Pt sites for further chemisorptions of methanol molecules, thus making the dehydrogenation of methanol molecules adsorbed on the Pt surface more effective [25–28]. Therefore, both of the greater metallic proportion of Pt and the hydrogen spillover from the Pt surface to the WO_x surface in the PtRu/WO_x catalyst promoted methanol dehydrogenation greatly. At 0.20 V, a new peak appears at 2343 cm^{-1}, which can be assigned to C–O stretching mode of CO_2, i.e., the final product for methanol electro-oxidation. Fig. 12 also shows integrated IR intensities of CO_2 generated on

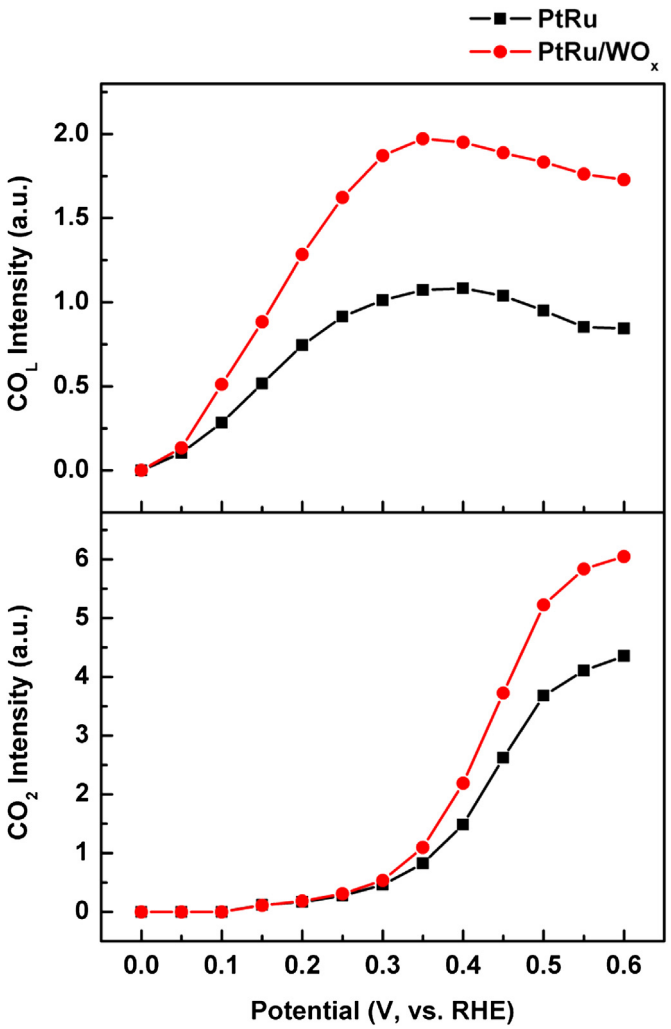

Fig. 12. Integrated IR intensities for CO_L and CO_2 generated on PtRu/WO_x and PtRu catalysts as a function of electrode potential.

the PtRu/WO_x and PtRu catalysts as a function of electrode potential. More CO_2 was formed on the PtRu/WO_x catalyst surface, indicating that CO_{ads} on the PtRu sites could be converted into CO_2 with a great rate. This result also agrees with those shown in Figs. 8–10 in the same solution.

4. Conclusions

PtRu/WO_x catalyst was prepared in a polyol process with 3DOM WO_3 template in combination with an ammonia-leaching treatment. STEM, EDX and N_2 adsorption results showed that the use of 3DOM WO_3 template prevented the agglomeration of PtRu nanoparticles and obtained a porous structure. XPS and XRD results indicated that both of the PtRu/WO_x and PtRu catalysts had a similar surface composition and crystalline structure, while there was about 4 at.% of WO_x in the PtRu/WO_x catalyst. The higher metallic Pt proportion in the PtRu/WO_x catalyst might be due to the interaction between the PtRu nanoparticles and WO_x. CO stripping voltammetry and *in situ* IRRAS results validated that the PtRu/WO_x catalyst had an improved CO_{ads} electro-oxidation and methanol dehydrogenation activities. The electrochemical measurements of methanol oxidation indicated that the use of 3DOM WO_3 template not only assisted the electro-catalytic reaction for methanol oxidation by the residual WO_x, but also benefitted the mass transport of methanol to the catalyst surface due to the porous structure.

Acknowledgments

This study was financially supported by Specialized Research Fund for the Doctoral Program of Higher Education of China (Grant No. 20122124120004) and the New Energy and Industrial Technology Development Organization (NEDO) of Japan.

References

[1] A.S. Aricò, S. Srinivasan, V. Antonucci, Fuel Cells 1 (2001) 133–161.
[2] M.P. Hogarth, T.R. Ralph, Platinum Metals Review 46 (2002) 146–164.
[3] C. Lim, R.G. Allen, K. Scott, Journal of Power Sources 161 (2006) 11–18.
[4] G.X. Wang, G.Q. Sun, Q. Wang, S.L. Wang, J.S. Guo, Y. Gao, Q. Xin, Journal of Power Sources 180 (2008) 176–180.
[5] Q. Mao, G.Q. Sun, S.L. Wang, H. Sun, G.X. Wang, Y. Gao, A.W. Ye, Y. Tian, Q. Xin, Electrochimica Acta 52 (24) (2007) 6763–6770.
[6] J.S. Guo, G.Q. Sun, S.G. Sun, S.Y. Yan, W.Q. Yang, J. Qi, Y.S. Yan, Q. Xin, Journal of Power Sources 168 (2007) 299–306.
[7] E. Antolini, J. Perez, Journal of Materials Sciences 46 (2011) 4435–4457.
[8] A. Kloke, F. von Stetten, R. Zengerle, S. Kerzenmacher, Advanced Materials 23 (2011) 4976–5008.
[9] H.J. Wang, M. Imura, Y. Nemoto, L. Wang, H.Y. Jeong, T. Yokoshima, O. Terasaki, Y. Yamauchi, Chemistry-A European Journal 18 (2012) 13142–13148.
[10] S.M. Choi, J.H. Kim, J.Y. Jung, E.Y. Yoon, W.B. Kim, Electrochimica Acta 53 (2008) 5804–5811.
[11] Z.W. Chen, M. Waje, W.Z. Li, Y.S. Yan, Angewandte Chemie-International Edition 46 (2007) 4060–4063.
[12] S.M. Alia, K.O. Jensen, B.S. Pivovar, Y.S. Yan, ACS Catalysis 2 (2012) 858–863.
[13] J.H. Jiang, A. Kucernak, Electrochemistry Communications 11 (2009) 623–626.
[14] L.N. Zhuang, W.J. Wang, F. Hong, S.C. Yang, H.J. You, J.X. Fang, B.J. Ding, Journal of Solid State Chemistry 191 (2012) 239–245.
[15] C.H. Cui, J.W. Yu, H.H. Li, M.R. Gao, H.W. Liang, S.H. Yu, ACS Nano 5 (2011) 4211–4218.
[16] S. Garbarino, A. Ponrouch, S. Pronovost, D. Guay, Electrochemistry Communications 11 (2009) 1449–1452.
[17] Z. Jusys, T.J. Schmidt, L. Dubau, K. Lasch, L. Jörissen, J. Garche, R.J. Behm, Journal of Power Sources 105 (2002) 297–304.
[18] J.L. Ye, J.G. Liu, Z.G. Zou, J. Gu, T. Yu, Journal of Power Sources 195 (2010) 2633–2637.
[19] G.X. Wang, T. Takeguchi, Y. Zhang, E.N. Muhamad, M. Sadakane, S. Ye, W. Ueda, Journal of The Electrochemical Society 156 (7) (2009) B862–B869.
[20] G.X. Wang, T. Takeguchi, T. Yamanaka, E.N. Muhamad, M. Mastuda, W. Ueda, Applied Catalysis B: Environmental 98 (2010) 86–93.
[21] M. Arenz, V. Stamenkovic, B.B. Blizanac, K.J. Mayrhofer, N.M. Markovic, P.N. Ross, Journal of Catalysis 232 (2005) 402–410.
[22] L.X. Yang, C. Bock, B. MacDougall, J. Park, Journal of Applied Electrochemistry 34 (2004) 427–438.
[23] C. Roth, M. Goetz, H. Fuess, Journal of Applied Electrochemistry 31 (2001) 793–798.
[24] C.Z. He, H.R. Kunz, J.M. Fenton, Journal of The Electrochemical Society 150 (2003) A1017–A1024.
[25] P.J. Barczuk, H. Tsuchiya, J.M. Macak, P. Schmuki, D. Szymanska, O. Makowski, K. Miecznikowski, P.J. Kulesza, Electrochemical and Solid-State Letters 9 (2006) E13–E16.
[26] K.-W. Park, J.-H. Choi, K.-S. Ahn, Y.-E. Sung, Journal of Physical Chemistry B 108 (2004) 5989–5994.
[27] F. Micoud, F. Maillard, A. Bonnefont, N. Job, M. Chatenet, Physical Chemistry Chemical Physics 12 (2010) 1182–1193.
[28] F. Maillard, E. Peyrelade, Y. Soldo-Olivier, M. Chatenet, E. Chaînet, R. Faure, Electrochimica Acta 52 (2007) 1958–1967.
[29] M. Sadakane, T. Horiuchi, N. Kato, C. Takahashi, W. Ueda, Chemistry of Materials 19 (23) (2007) 5779–5785.
[30] M. Sadakane, K. Sasaki, H. Kunioku, B. Ohtani, W. Ueda, R. Abe, Chemical Communications (2008) 6552–6554.
[31] M. Sadakane, K. Sasaki, H. Kunioku, B. Ohtani, R. Abe, W. Ueda, Journal of Materials Chemistry 20 (2010) 1811–1818.
[32] Q. Wang, G.Q. Sun, L.H. Jiang, Q. Xin, S.G. Sun, Y.X. Jiang, S.P. Chen, Z. Jusys, R.J. Behm, Physical Chemistry Chemical Physics 9 (2007) 2686–2696.
[33] G.X. Wang, T. Takeguchi, E.N. Muhamad, T. Yamanaka, W. Ueda, International Journal of Hydrogen Energy 36 (2011) 3322–3332.
[34] E.A. Anumol, A. Halder, C. Nethravathi, B. Viswanath, N. Ravishankar, Journal of Material Chemistry 21 (2011) 8721–8726.
[35] D.L. Wang, L. Zhuang, J.T. Lu, Journal of Physical Chemistry C 111 (2007) 16416–16422.
[36] A. Lewera, L. Timperman, A. Roguska, N. Alonso-Vante, The Journal of Physical Chemistry C 115 (2011) 20153–20159.
[37] L. Colmenares, H. Wang, Z. Jusys, L. Jiang, S. Yan, G.Q. Sun, R.J. Behm, Electrochimica Acta 52 (2006) 221–233.
[38] V. Radmilović, H.A. Gasteiger, P.N. Ross Jr., Journal of Catalysis 154 (1995) 98–106.
[39] K.A. Friedrich, K.P. Geyzers, A.J. Dickinson, U. Stimming, Journal of Electroanalytical Chemistry 524-525 (2002) 261–272.
[40] S. Park, A. Wieckowski, M.J. Weaver, Journal of the American Chemical Society 125 (2003) 2282–2290.
[41] F. Maillard, G.Q. Lu, A. Wieckowski, U. Stimming, Journal of Physical Chemistry B 109 (2005) 16230–16243.
[42] M. Metikoš-Hukovic, R. Babic, Y. Piljac, Journal of New Materials for Electrochemical Systems 7 (2004) 179–190.